

LOAD-BEARING CAPACITY OF TEMPERED STRUCTURAL GLASS

By H el ene Carr e¹ and L. Daudeville²

ABSTRACT: This paper presents a method for the failure analysis of structural glass components of buildings. Structural glass is generally prestressed by tempering. In the method, residual stresses are first computed by simulation of this tempering process of soda-lime-silica glass plates using the finite-element method. The model includes both stress and structural relaxations. The edge effects of tempering are modeled. Then, the failure strength of annealed glass is obtained by a statistical analysis of tests performed on small specimens. Loading rate effects are also taken into account. Computational results are associated with the statistical approach for the failure prediction of large annealed and tempered glass plates. This prediction method is validated by experimental results from four-point bending tests up to failure.

INTRODUCTION

New applications of tempered glass in structural parts of buildings (i.e., posts, beams, and shear walls) necessitate a good knowledge of the load-carrying capacity and the lifetime of structural glass components. The objective of this work is the strength prediction of tempered soda-lime-silica glass plates loaded in plane.

Tempered glass may be regarded as a prestressed material because its thermal treatment induces a certain amount of residual stresses. As these stresses are hardly measurable at all points of an element, simulation of the tempering process is necessary to evaluate the transient and residual stress states. Previous studies of tempering have been concerned with the calculation of residual stresses in infinitely thin plates (Narayanan and Gardon 1969; Gardon 1980; Burke et al. 1987; Carr e and Daudeville 1996). Knowledge of the 3D stress state in the whole plate is necessary as catastrophic failure is the consequence of the propagation of cracks originated by machining the edges of glass plates (i.e., the influence of volume defects being neglected). Because of the present scarcity of knowledge of the state of residual stresses near straight edges or holes, full-scale tests are generally necessary to design tempered glass elements. The 3D calculation of residual stresses near edges has not been shown before.

In this paper, computational results of the 3D finite-element (FE) simulation of tempering of a thick glass plate are first presented. Because failure properties of glass during the various stages of solidification are unknown, transient stresses have possible application only in controlling the quenching process and the resulting residual stresses.

Then, experimental results of four-point bending (FPB) tests performed on small annealed glass specimens are shown. The strength distribution and static fatigue sensitivity are determined from tests under constant stress rates. The influences of the loading rate and surface finish are investigated. Tests were performed in usual moisture conditions (i.e., the influence of the relative humidity was not studied).

For a reliable failure analysis of glass elements, the Weibull (1951) model is identified from tests performed on the small annealed specimens. The loading rate effect is included in the Weibull model by means of fracture mechanics concepts.

The goal of this paper is strength prediction of large structural elements. The origin of fracture in structural glass is via mechanical damage due to machining that involves abrading the surface. The initial size of edge scratches is between 10 and 100 μm . Their final size before catastrophic propagation is of the same order of magnitude for annealed glass or tempered glass under flexion. The stress state of tempered plates under bending can then be considered as quasi-uniform in the vicinity of edge cracks. The analysis is different from the problem of nonloaded tempered glass objects (notably automobile windshields) containing clearly visible surface cracks in which the variation of stresses along the crack must be taken into account.

A superposition model is proposed for the strength prediction of tempered glass plates. The model uses results from the numerical simulations of tempering and data from the probabilistic model of the studied glass with machined cracks. The main assumptions can be debated, but the simplified model must be considered as a first step. Some FPB tests were performed up to failure on large annealed and tempered elements. Experiments on annealed specimens confirm the ability of the statistical model to describe the size effect. Another original aspect of the paper is the use of optical measurements on large tempered specimens that allow the identification of unknown heat transfer parameters of the tempering process and the validation of the FE model. Failure tests validate the superposition method and the Weibull model.

THERMAL TEMPERING SIMULATION

Thermal tempering of glass consists of cooling very quickly, by air casts, a plate that has been heated to $\sim 620^\circ\text{C}$. This treatment confers a strengthening by means of a residual stress state of tension in the core and of compression near the surface. The goal of FE simulations of quenching is to obtain residual stresses of thick tempered soda-lime-silica glass plates.

The present difficulty of such a problem is the correct modeling of heat transfers particularly in the case of a complex geometry (e.g., a holed plate). Obtaining reliable data of the thorough Narayanan (1978) model used in this study is another difficulty. Available data in this paper are issued from experimental studies carried out at Saint-Gobain Recherche, Aubervilliers, France.

Thermomechanical Behavior of Glass

The behavior varies quickly around the transition temperature ($T_g \approx 580^\circ\text{C}$) between the "glass" and "liquid" states. The presented model includes stress relaxation due to viscosity and structural relaxation due to the actual state of structure of glass. The viscous behavior can be neglected at 20°C .

Mechanical Behavior

Temperature is first considered constant. The mechanical behavior of glass is described in terms of stress relaxation by

¹Res. Engr., Ctr. Scientifique et Technique du B atiment, 84 Ave. Jean Jaur es, 77421 Marne-la-Vall ee Cedex 02, France.

²Assoc. Prof., Laboratoire de M ecanique et Technologie, Ecole Normale Sup erieure de Cachan/CNRS/Universit  Paris 6, 61 Ave. du Pr esident Wilson, 94235 Cachan Cedex, France; corresponding author.

Note. Associate Editor: Gilles Pijaudier-Cabot. Discussion open until January 1, 2000. To extend the closing date one month, a written request must be filed with the ASCE Manager of Journals. The manuscript for this paper was submitted for review and possible publication on November 25, 1997. This paper is part of the *Journal of Engineering Mechanics*, Vol. 125, No. 8, August, 1999.  ASCE, ISSN 0733-9399/99/0008-0914-0921/\$8.00 + \$.50 per page. Paper No. 17123.

means of a generalized Maxwell model (Duffrene 1994; Gy et al. 1994). Relaxation shear and bulk moduli are described with instantaneous and deferred moduli and expanded into Prony's series. The deferred shear modulus value is zero

$$G(t) = 2G_g\Psi_1(t) \quad (1)$$

$$K(t) = 3K_e - (3K_e - 3K_g)\Psi_2(t) \quad (2)$$

$$\Psi_i(t) = \sum_{j=1}^{n_i} w_{ij} \exp\left(-\frac{t}{\tau_{ij}}\right), \quad i = 1, 2 \quad (3)$$

Influence of Temperature

A relaxation function $\Psi_i(T)$ known at the reference temperature T_{ref} can be determined at any temperature T with a classical time-temperature equivalence (Schwarzl and Staverman 1952) by means of the reduced time ξ defined as

$$\Psi_i(T, t) = \Psi_i(T_{ref}, \xi), \quad i = 1, 2 \quad (4)$$

Weights and relaxation times, defined in (3), are assumed

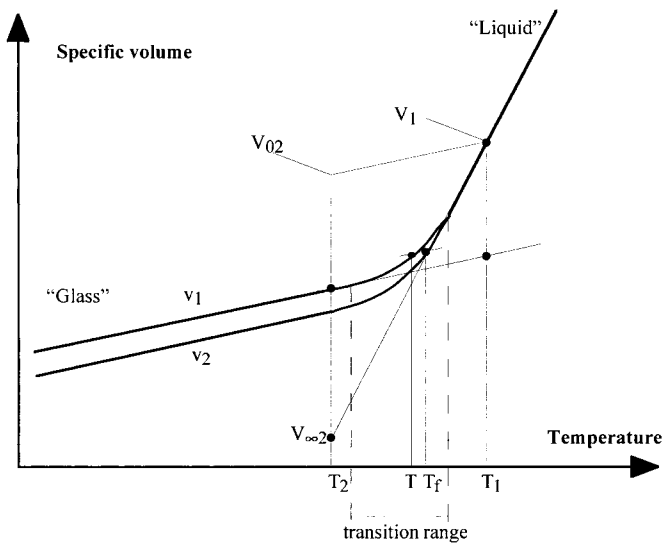


FIG. 1. Specific Volume versus Temperature and Definition of Fictitious Temperature

constant with temperature. An Arrhenius relation allows a correct description of the dependency of relaxation times with temperature (Narayanaswamy 1978; Gardon 1980)

$$\xi(t, T) = \int_0^t \exp\left(-\frac{H}{R}\left(\frac{1}{T_{ref}} - \frac{1}{T(t')}\right)\right) dt' \quad (5)$$

Structural Relaxation

During the quenching, and for temperatures close to the transition range, the glass structure cannot be stabilized. There are several possible glassy states for one temperature depending on the cooling rate (Fig. 1). This is the structural relaxation (Narayanaswamy and Gardon 1969; Narayanaswamy 1971).

The fictitious temperature T_f was introduced to account for the structure of glass (Tool 1946). A structural relaxation volume function M_v is defined as follows (Fig. 1):

$$M_v(t) = \frac{V(t) - V_{\infty,2}}{V_{0,2} - V_{\infty,2}} = \frac{T_f - T_2}{T_1 - T_2} \quad (6)$$

Its temperature dependency is taken into account with the reduced time $\xi(t)$. The fictitious temperature T_f is defined as

$$T_f(t) = T(t) - \int_0^t M_v[\xi(t) - \xi(t')] \frac{dT(t')}{dt'} dt' \quad (7)$$

By analogy with the viscous relaxation, the response function can be described with a Prony's series

$$M_v(\xi) = \sum_{i=1}^n C_i \exp\left(-\frac{\xi}{\lambda_i}\right) \quad (8)$$

Structural relaxation times λ_i are considered to be proportional to shear relaxation times (Guillemet et al. 1992).

The dependency of viscosity with the structure state is not considered in the presented FE simulations because it induces very small variations of residual stresses (Gardon 1980). However, the dependency of the structural state with the density, which is much more significant on residual stresses, is introduced by means of the thermal expansion coefficient variations with the temperature

$$\varepsilon_{th} = \beta_g(T(t) - T_f(t)) + \beta_l(T_f(t) - T_0) \quad (9)$$

TABLE 1. Thermoviscoelastic Characteristics

Young's modulus E (1)	Poisson ratio ν (2)	K_g/K_g [Eq. (2)] (3)	H/R [Eq. (5)] (4)	β_g [Eq. (9)] (5)	β_l [Eq. (9)] (6)
70 GPa	0.22	0.18	55,000 K	$9 \times 10^{-6} \text{ }^\circ\text{C}^{-1}$	$25 \times 10^{-6} \text{ }^\circ\text{C}^{-1}$

TABLE 2. Viscous and Structural Relaxations—Weights and Relaxation Times ($T_{ref} = 864 \text{ K}$)

i (1)	$w_{1i}G_g$ (GPa) (2)	τ_{1i} (s) (3)	$w_{2i}K_g$ (GPa) (4)	τ_{2i} (s) (5)	C_i (6)	λ_i (s) (7)
1	1.5845	6.658×10^{-5}	0.7588	5.009×10^{-5}	5.523×10^{-2}	5.965×10^{-4}
2	2.3539	1.197×10^{-3}	0.7650	9.945×10^{-4}	8.205×10^{-2}	1.077×10^{-2}
3	3.4857	1.514×10^{-2}	0.9806	2.022×10^{-3}	1.215×10^{-1}	1.362×10^{-1}
4	6.5582	1.672×10^{-1}	7.301	1.925×10^{-2}	2.286×10^{-1}	1.505
5	8.2049	7.497×10^{-1}	13.47	1.199×10^{-1}	2.860×10^{-1}	6.747
6	6.4980	3.292	10.896	2.033	2.265×10^{-1}	29.63

TABLE 3. Thermal Conductivity and Specific Heat

Thermal conductivity λ (W/m·K, T in $^\circ\text{C}$) (1)	Specific heat of liquid glass $C_{p,l}$ (J/kg·K, T in K) (2)	Specific heat of glass $C_{p,g}$ (J/kg·K, T in K) (3)
$0.975 + 8.58 \times 10^{-4}T$	$1,433 + 6.5 \times 10^{-3}T$	$893 + 0.4T - 1.8 \times 10^{-7}T^2$

Glass Characteristics

The thermoviscoelastic characteristics (Duffrene 1994) are given in Tables 1 and 2. The structural relaxation characteristics (Guillemet et al. 1992) are in Table 2.

The thermal conductivity and the specific heat (Guillemet et al. 1992) are characteristics varying with temperature as shown in Table 3.

FE Analysis

Previous works investigated inner residual stresses of thin plates (thickness of 0.61 cm) (Narayanaswamy 1978; Gardon 1980; Burke et al. 1987; Carré and Daudeville 1996). This work concerns thick tempered glass plates of building structures loaded in plane. The origin of fracture is located on the plate edges. Therefore, transient and residual stresses are analyzed in both inner and edge zones with the FE code MARC. All of the following results are related to large tempered plates ($2,000 \times 300 \times 19 \text{ mm}^3$).

Mesh and Boundary Conditions

Although the problem does not depend on z , 3D elements are used to account for thermal strain along this coordinate

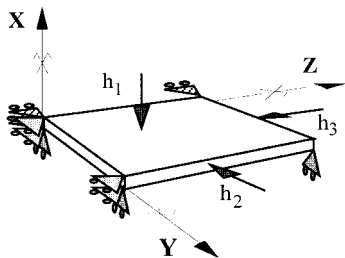


FIG. 2. FE Model

TABLE 4. Identification of Unknown Heat Transfer Coefficients

Coefficients (1)	Epibiascope (2)	Babinet compensator (3)
Mean measurement (MPa)	120.4	72
Standard deviation (MPa)	4.9	3.3
Apparatus accuracy (MPa)	± 6	± 1.2
Identification of h_1 and h_2 ($\text{W/m}^2 \cdot \text{K}$)	$h_1 = 135$	$h_2 = 115$

(Fig. 2). The mesh is refined in zones of high stress gradients, in the plate thickness (along x) and close to the edge (along y).

The thermal treatment is assumed to be uniform on all plate faces. The mechanical boundary conditions are symmetry conditions (i.e., only one-eighth of the plate is modeled). The thermal boundary conditions are forced convections to model the blowing by air casts (air temperature $T_{ext} = 20^\circ\text{C}$). Three constant heat transfer coefficients h_1 , $h_2 = h_3$ are defined. The plate temperature is assumed to be uniform and equal to T_0 (620°C) at the beginning of cooling.

The problem to solve is a time-dependent problem because of the viscous behavior of glass.

Identification of Heat Transfer Coefficients

The only unknown parameters of the tempering process simulation are the two heat transfer coefficients h_1 and h_2 . They are identified by means of comparisons between simulation results and optical measurements (Sinha 1978; Aben and Guillemet 1993; Redner 1995) of residual stresses performed on large tempered plates.

The "epibiascope" is used to obtain the surface stress ($\sigma_{yy} = \sigma_{zz}$) in several points in the inner part of the plate. This measurement allows the identification of h_1 (Table 4).

The "Babinet compensator" measures the difference of the optical path in the thickness of the plate that is proportional to the integral in the thickness t of the difference of principal stresses ($1/t \int_{-t/2}^{+t/2} (\sigma_{yy} - \sigma_{zz}) dx$). One measurement is carried out close to the edge to identify h_2 (Table 4, at 1.5 mm because of the chamfer, point A of Fig. 3).

Several measures at different distances from the edge were carried out. The comparison between measurements and numerical simulations with the distance from the edge are given in Fig. 3. The good comparison validates the FE calculations of residual stresses.

Transient and Residual Stresses

At the beginning of cooling, the surface contracts more quickly than the core. By equilibrium, the core is under compression and the surface is under tension. The surface tension, particularly important at the beginning of cooling at the plate corner, may lead to the fracture of the tempered glass plate. As the surface temperature becomes less than the transient temperature, the surface freezes and the still liquid core con-

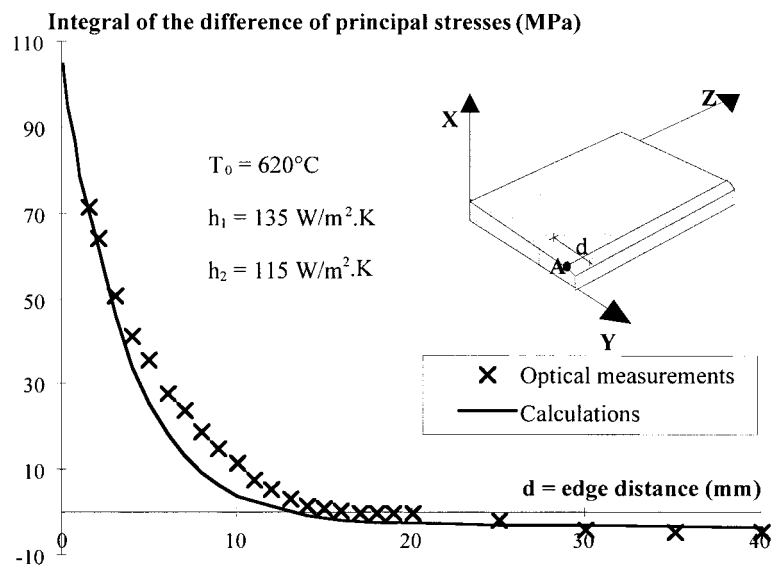


FIG. 3. Integral of Difference of Principal Stresses versus Distance from Edge

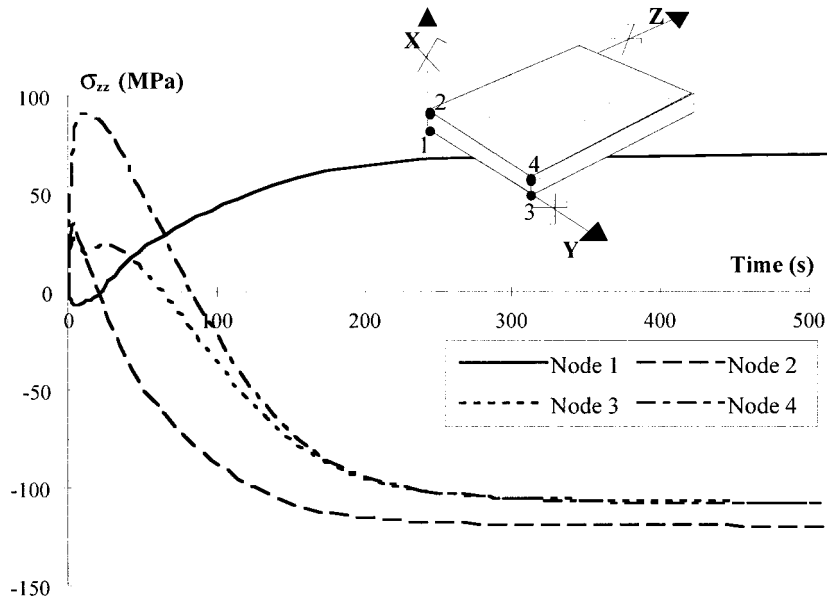


FIG. 4. Computed Stress Variation versus Time at Edge and in Inner Part of Plate

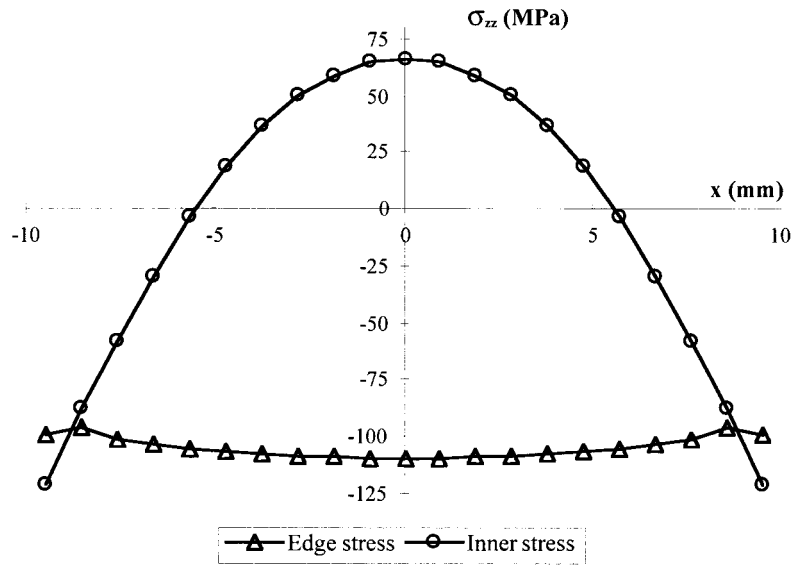


FIG. 5. Computed Stress Variation versus Thickness Coordinate at Edge and in Inner Part of Plate

tinues to contract. Then, the surface becomes compressed while the core is under tension, by equilibrium (Fig. 4).

In the inner part of the plate, the residual stress $\sigma_{yy} = \sigma_{zz}$ has a parabolic shape in the plate thickness. The residual edge stress σ_{zz} is quasi-constant in the thickness and slightly less than the inner surface stress (Fig. 5).

FRACTURE PARAMETERS IDENTIFICATION

The failure stress of a macroscopic annealed glass element under tension is between 30 and 100 MPa, whereas the tensile strength of a glass fiber is about 20 GPa. Griffith (1920) explained this by the presence of microcracks. The origin of fracture is located on the machined edges. Failure is governed on one hand by their propagation and on the other hand by their random distribution.

Statistical Model

The Weibull (1951) model is a statistical approach for the failure analysis of brittle materials with random defects. The failure probability P_f of a glass plate is

$$P_f = 1 - \exp \left[-\frac{1}{S_0} \int_S \left(\frac{\sigma - \sigma_u}{\sigma_0} \right)^m \right] \quad (10)$$

This model accounts for the size effect and the stress concentration effect. Weibull parameters depend on the material and also on the loading rate because of the subcritical crack growth.

For a glass plate under bending, S is the polished surface under tension. The integration of (10) on S is then explicit. It was verified for each test presented in the next sections that cracking had originated on S and not below the surface (for annealed or tempered glass specimens).

Subcritical Crack Growth

Glass strength depends on the rate and the duration of loading. This phenomenon, also named static fatigue, was shown by Grenet (1899). This is not observed in vacuum conditions, and it is due to the effect of moisture at the crack tips (Michalske and Freiman 1983).

Failure due to the propagation of cracks from the edge can be modeled by means of the stress intensity factor (SIF) K_I of

fracture mechanics. Glass is a brittle material, and so the fracture mode can be considered as a pure mode I. The crack velocity depends on K_I (Wiederhorn 1967) because of the subcritical crack growth. Evans (1974) proposed the following model:

$$K_I < K_{Ith} \quad \text{no crack propagation} \quad (11a)$$

$$K_{Ith} \leq K_I < K_{Ic} \quad \text{subcritical crack growth: } \frac{da}{dt} = AK_I^n \quad (11b)$$

$$K_{Ic} \leq K_I < K_{Icb} \quad \text{crack propagation} \quad (11c)$$

$$K_I = K_{Icb} \quad \text{crack branching} \quad (11d)$$

The SIF is calculated with the applied stress (far away from the crack)

$$K_I = \sigma Y \sqrt{\pi a} \quad (12)$$

The shape factor can be issued from Rooke and Cartwright (1976).

Identification Tests

Description of Tests

Small annealed specimens with polished edges were tested under FPB with different loading rates (Fig. 6). The influences of the loading rate and the surface finish were studied. The first set of specimens was tested at 0.05 and 0.5 MPa/s under displacement control. Then a second set of specimens, with a different surface finish, was tested at 0.05, 0.5, and 5 MPa/s.

The reference surface finish is the first one because large specimens described further were machined with this surface finish.

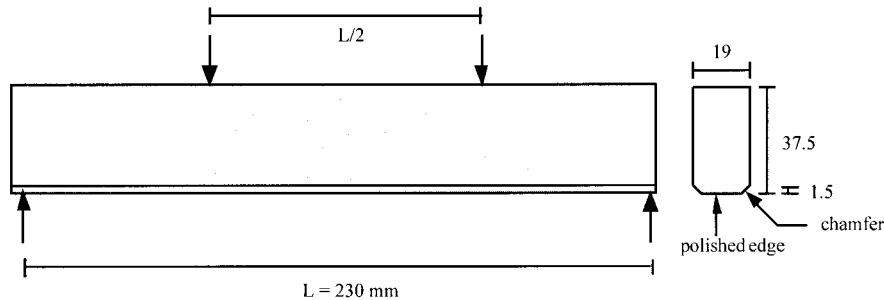


FIG. 6. FPB Test on Small Specimens

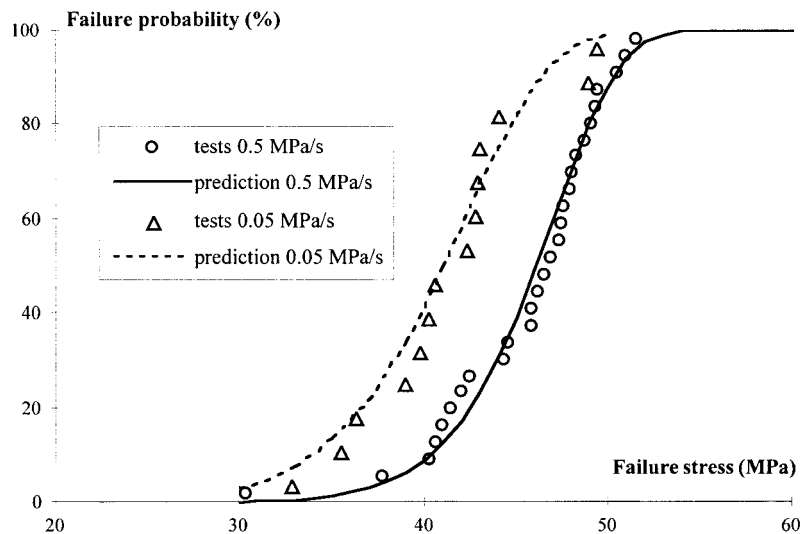


FIG. 7. Predictions with Weibull Model

In Fig. 7, circles and triangles give, for the reference surface finish and for all the tested specimens, the experimental cumulative failure probabilities at 0.05 and 0.5 MPa/s with respect to the applied stress on the tensile edge. It can be observed, first, that there is a large scattering of the failure stress justifying a statistical approach and, second, that there is an influence of the loading rate.

Table 5 gives the experimental mean failure stress and the two experimental stresses corresponding to failure probabilities of 0.2 and 0.8. Results are very different for the two qualities of machining.

Loading Rate Effect

Association of the Weibull and Evans models enables one to account for the subcritical crack growth in the statistical analysis. The apparent Weibull parameters (σ_0 and m) depend on both the loading rate and the environment for a given surface finish. Intrinsic parameters (m^* and σ_0^*) are defined from the strength in inert medium.

Assuming $\sigma_u = 0$ and $S_0 = 1$, (10) gives for a FPB test in inert medium

$$P_f = 1 - \exp \left[-S \left(\frac{\sigma_i}{\sigma_0^*} \right)^{m^*} \right] \quad (13)$$

Intrinsic Weibull parameters (σ_0^* and m^*) are independent of the loading conditions. The failure probability for a constant stress or stress rate can be written with the intrinsic parameters and the subcritical crack growth parameters (Helfinstine 1980; Carré 1996).

Assuming the initial defect length is small compared with the final crack length [$a(t=0) \ll a(t=t_f)$] and that the value of the threshold stress intensity factor is zero ($K_{Ith} = 0$), the integration of (11) in time, (12) and (13) give

TABLE 5. Experimental Failure Stresses of Small Specimens

Failure stress (MPa) (1)	$\dot{\sigma}$ (MPa/s)		
	0.05 (2)	0.5 (3)	5 (4)
(a) First surface finish			
$P_f = 0.2$	37.0	41.5	—
Mean	41.2	45.4	—
$P_f = 0.8$	43.7	49.1	—
(b) Second surface finish			
$P_f = 0.2$	39.9	45.1	45.2
Mean	50.1	54.7	56.1
$P_f = 0.8$	57.2	64.0	66.2

$$P_f = 1 - \exp \left[-S \left(\frac{\sigma}{\sigma_0} \right)^m \right]$$

$$= 1 - \exp \left[-S \left(\frac{\sigma}{\sigma_0^*} \right)^{nm^*/(n-2)} \left(\frac{t_f}{t^*} \right)^{m^*/(n-2)} k(n) \right] \quad (14)$$

with

$$t^* = \frac{2}{n-2} \frac{1}{AY^2} \sigma_0^{*2} K_{Ic}^{2-n} \quad (15)$$

The factor $k(n)$ depends on the loading rate

$$k(n) = \begin{cases} 1 & \text{if } \dot{\sigma} = 0 \\ \left(\frac{1}{n+1} \right)^{m^*/(n-2)} & \text{if } \dot{\sigma} = \text{const} \end{cases} \quad (16)$$

Then, the apparent Weibull parameters are

$$m = \frac{(n+1)m^*}{n-2} \quad (17)$$

$$\sigma_0 = (\sigma_0^*)^{(n-2)/(n+1)} \left(\dot{\sigma} \frac{2(n+1)}{(n-2)AY^2 K_{Ic}^{n-2}} \right)^{1/n} \quad (18)$$

Only the apparent Weibull stress σ_0 depends on the stress rate. If the initial crack length is not neglected, the two apparent Weibull parameters (m and σ_0) depend on the loading rate (Carré 1996).

Determination of Weibull Parameters

Apparent Weibull parameters (m and σ_0)_{0.5} were identified with the test results shown in Fig. 7 obtained at a stress rate of 0.5 MPa/s. The maximum likelihood method was used for the identification (continuous line in Fig. 7).

The apparent Weibull parameters at 0.05 MPa/s can be calculated with (17) and (18). It should be noticed that the knowledge of fracture mechanics parameters, A , Y , and K_{Ic} is not necessary because the calculation of the intrinsic Weibull stress σ_0^* is not carried out

$$(m)_{0.05} = (m)_{0.5}; \quad (\sigma_0)_{0.05} = (\sigma_0)_{0.5} \left(\frac{0.05}{0.5} \right)^{1/n} \quad (19a,b)$$

The failure prediction at 0.05 MPa/s is given by a dashed line in Fig. 7. The correct prediction validates the association of the subcritical crack growth model with the Weibull theory. The only fracture mechanics parameter used in this study is the exponent n . This material parameter is difficult to obtain because it requires long-term observations of crack propagation. For usual moisture conditions in buildings, n was identified from double torsion tests ($n = 12.76$, private communication from R. Gy, Saint-Gobain Recherche, 1995).

STRENGTH PREDICTION OF TEMPERED GLASS ELEMENTS

In one case, numerical simulations of glass tempering have given the residual stress state of thick plates. In another case, tests on small annealed glass samples have allowed the identification of statistical failure parameters of the studied glass.

The strength prediction of tempered glass elements will now be proposed by associating the two previous analyses.

Superposition Method

A key point is that the crack length before failure can be considered small compared with the lengths of stress variation. Fig. 8 gives the residual stress parallel to the edge with respect to the edge distance in the midplane of a large tempered plate. The zoomed image shows that the residual stress can be considered as constant along a distance that is about one crack length before failure (about 100 μm) (Carré 1996).

The study of a clearly visible crack would involve taking

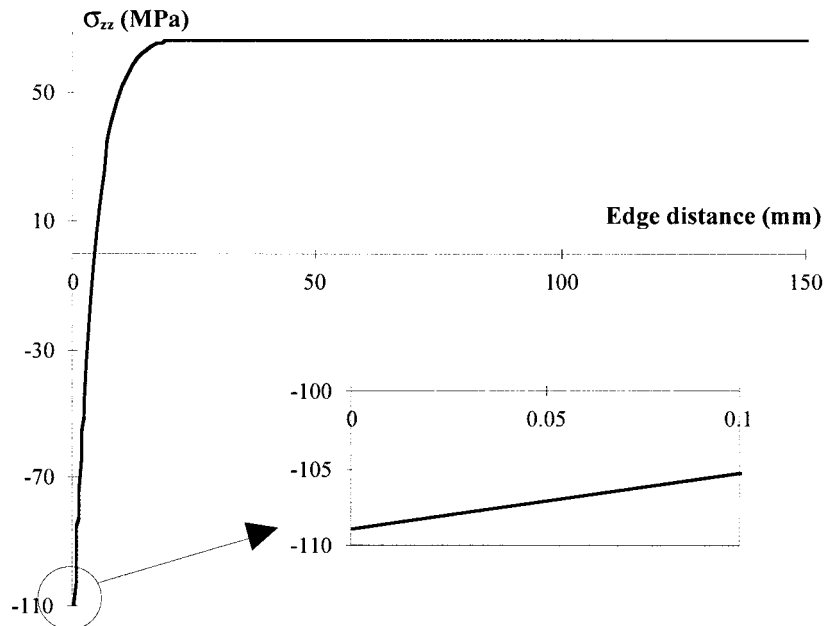


FIG. 8. Residual Stress Parallel to Edge versus Edge Distance

into account the variation of stress along the crack length (Lawn and Marshall 1977). Here, in the studied problem, the crack does not grow through a region of negative K_I (due to a residual stress of compression) to a region of positive K_I for a long crack length because the crack will not propagate as long as the whole crack is in a region under compression.

The stress state (i.e., the superposition of residual and bending stresses) can be considered as uniform far away from the crack. Then, a crack propagation will be possible when the sum of the bending and residual stress values reaches a critical value.

The strength prediction is based on the following two major assumptions:

- Residual stresses due to tempering are deterministic data. This assumption relies on the observation of a small dispersion shown from optical measurements of residual stresses on several points of different glass plates tempered in the same conditions (Table 4).
- The surface flaw distribution is not affected by tempering in spite of a surface tension stress at the beginning of the cooling process that may induce a crack propagation.

The superposition method gives (at the location of failure)

tempered glass strength (T)

$$= \text{annealed glass strength (A)} + \text{residual stress (R)} \quad (20)$$

(Weibull model) (FE simulation)

Tests on Large Glass Elements

Large annealed and tempered glass plates ($2,000 \times 300 \times 19 \text{ mm}^3$) were tested under FPB at 0.05 MPa/s (Fig. 9). This system prevents the plates from lateral bending. It was verified that this system does not induce any out-of-plane bending stresses with gauges on each face of the plate. The edges of large and small elements were machined in the same conditions (first surface finish).

Annealed Specimens

In a first step, the Weibull model is used for the failure probability prediction of large annealed glass plates. The aim is the verification of the size effect description. The strength predictions for three probabilities of failure are obtained with (14)–(19) [term A in (20)] and are given in Table 6. The size effect is clearly shown by comparing Tables 5 and 6.

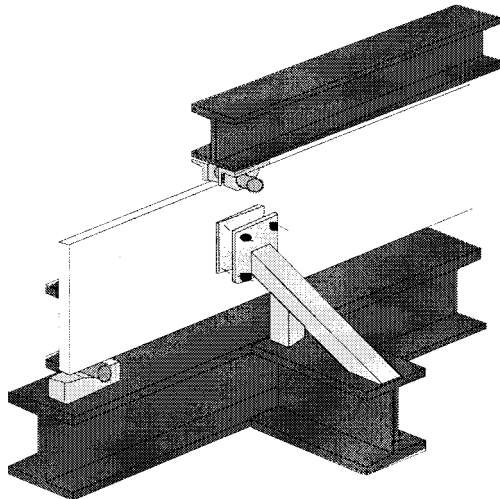


FIG. 9. Half Perspective of Experimental Setup for Large Specimens

TABLE 6. Failure Stresses of Large Annealed and Tempered Specimens ($\dot{\sigma} = 0.05 \text{ MPa/s}$)

Failure stress (MPa) (1)	Annealed glass (2)	Tempered glass (3)
Average of tests	31.3	126.8
Prediction		
$P_f = 0.2$	30.7	126.7
Mean ($P_f = 0.44$)	33	129.0
$P_f = 0.8$	35.5	141.5

According to the model, the mean experimental failure stress σ_{exp} corresponds to a failure probability of 0.26. The small difference (5%) between the mean experimental and predicted failure stresses may be due to the influence of n [(19)] whose value is difficult to obtain.

Tempered Specimens

In a second step, the strength prediction of tempered glass plates [term T in (20)] is compared with experimental results. The minimum residual compression stress obtained on the edge by FE calculation [term R in (20)] is 96 MPa (Fig. 5). This stress was obtained near the chamfer. Calculated failure stresses are given in Table 6.

The difference between the mean experimental and calculated failure stress of tempered plates (2%) may be due to the influence of n but also on the uncertainty in the identification of the heat transfer coefficients (Table 4) due to the apparatus accuracy.

CONCLUSIONS

The FE simulation of thermal tempering of a soda-lime-silica glass plate was presented. Previous studies have not considered edge effects of tempering. A 3D analysis is carried out in the vicinity of the edge plate where optical measurements cannot give direct accurate estimations of residual stresses. It was proposed to identify the unknown heat transfer coefficients by means of a few optical measurements on the edge and in the center part of the plate that give some information on residual stresses in these regions. This approach can be applied to more complex geometries such as holes.

Tests on small annealed glass samples allow the determination of statistical annealed glass failure parameters and pointed out the loading rate effect. The probabilistic model of Weibull is used in association with a subcritical crack growth model. For a given surface finish, the model can take into account the effects of the specimen size of the stress distribution and of the rate of loading.

With the results of both previous models, the superposition method allows the strength prediction of large tempered glass elements. This method is validated by the comparison between experimental and calculated failure strengths.

The extrapolation of presented results to structural glass elements of buildings loaded on a long period must be validated. Long term FPB tests are now in process at Centre Scientifique et Technique du Bâtiment, Marne-la-Vallée, France.

ACKNOWLEDGMENTS

The writers would like to thank J. Mazars of Ecole Normale Supérieure de Cachan and C. Balloche from Centre Scientifique et Technique du Bâtiment for giving advice and R. Gy from Saint-Gobain Recherche for advice and specimens.

APPENDIX I. REFERENCES

- Aben, H., and Guillemet, C. (1993). *Photoelasticity of glass*. Springer, Berlin.
- Burke, M. A., Soules, T. F., Busbey, R. F., and Kheson, S. M. (1987). "Finite-element calculation of stresses in glass parts undergoing vis-

cous relaxation." *J. Am. Ceramic Soc.*, 70(2), 90–95.

Carré, H. (1996). "Etude d'un matériau fragile précontraint: le verre trempé," PhD thesis, Ecole Nationale des Ponts et Chaussées, Champs-sur-Marne, France (in French).

Carré, H., and Daudeville, L. (1996). "Numerical simulation of soda-lime silicate glass tempering." *J. de Physique IV, Colloque C1*, 6, 175–185.

Duffrene, L. (1994). "Comportement viscoélastique d'un verre silico-sodocalcique dans le domaine des températures intermédiaires," PhD thesis, Ecole Nationale Supérieure des Mines de Paris, Paris (in French).

Evans, A. G. (1974). "Slow crack growth in brittle materials under dynamic loading conditions." *Int. J. Fracture*, 10(2), 251–259.

Gardon, R. (1980). "Thermal tempering of glass." *Glass: Science and technology*, D. R. Uhlmann and N. J. Kreid, eds., Academic, New York.

Grenet, L. (1899). "Mechanical strength of glass." *Bull. Soc. Enc. Nat.*, Paris, 5(4), 838–848.

Griffith, A. (1920). "The phenomena of rupture and flow in solids." *Philosophical Trans. Royal Soc.*, London, A221, 163–198.

Guillemet, C., Gy, R., Labrot, M., Sipp, A., and Neuville, P. (1992). "Viscosity, configurational entropy and structural relaxation of soda-lime-silica glass." *Proc., 16th Int. Congr. of Glass*.

Gy, R., Duffrene, L., and Labrot, M. (1994). "New insights into the viscoelasticity of glass." *J. Non-Cryst. Solids*, 175, 103–117.

Helfinstine, J. D. (1980). "Adding static and dynamic fatigue effects directly to the Weibull distribution." *J. Am. Ceramic Soc.*, 63(1–2), 113–125.

Lawn, B. R., and Marshall, D. B. (1977). "Contact fracture resistance of physically and chemically tempered glass plates: a theoretical model." *Phys. and Chem. of Glasses*, 18(1), 7–18.

Michalske, T. A., and Frieman, S. W. (1983). "A molecular mechanism for stress corrosion in vitreous silica." *J. Am. Ceramic Soc.*, 66(4), 284–288.

Narayanaswamy, O. S. (1971). "A model of structural relaxation in glass." *J. Am. Ceramic Soc.*, 54(10), 491–498.

Narayanaswamy, O. S. (1978). "Stress and structural relaxation in tempering glass." *J. Am. Ceramic Soc.*, 61(3), 146–152.

Narayanaswamy, O. S., and Gardon, R. (1969). "Calculation of residual stresses in glass." *J. Am. Ceramic Soc.*, 52(10), 554–558.

Redner, A. S. (1995). "Back to basics: Nondestructive evaluation using polarized light." *Mat. Evaluation*, 53(6), 642.

Rooke, D. P., and Cartwright, D. J. (1976). *Compendium of stress intensity factors*. Hillington Press, Uxbridge Middlesex, England.

Schwarzl, F., and Staverman, A. J. (1952). "Time-temperature dependence of linear viscoelastic behavior." *J. Appl. Phys.*, 23(8), 838–843.

Sinha, N. K. (1978). "Stress state in tempered glass plate and determination of heat-transfer rate." *Experimental Mech.*, 18(1), 25–34.

Tool, A. Q. (1946). "Relation between inelastic deformability and thermal expansion of glass in its annealing range." *J. Am. Ceramic Soc.*, 29(9), 240–253.

Weibull, W. A. (1951). "A statistical distribution function of wide applicability." *J. Appl. Mech.*, 18, 293–297.

Wiederhorn, S. M. (1967). "Influence of water vapor on crack propagation in soda-lime silicate glass." *J. Am. Ceramic Soc.*, 50(8), 407–417.

APPENDIX II. NOTATION

The following symbols are used in this paper:

A = Evans's parameter;
a = crack length;

C_i = weights in structural relaxation function;
 $C_{p,g}$ = specific heat of solid glass;
 $C_{p,l}$ = specific heat of liquid glass;
G = shear modulus;
 G_g = instantaneous shear modulus;
H = energy of activation;
 h_i = heat transfer coefficients;
K = bulk modulus;
 K_e = deferred bulk modulus;
 K_g = instantaneous bulk modulus;
 K_I = SIF;
 K_{Ic} = critical SIF;
 K_{Icb} = crack branching SIF;
 K_{Ith} = threshold SIF;
 M_v = structural relaxation volume function;
m = apparent Weibull modulus;
 m^* = intrinsic Weibull modulus;
n = Evans's exponent;
 P_f = failure probability;
R = perfect gas constant;
S = area of possible location of fracture;
 S_0 = reference area;
T = temperature;
 T_f = fictitious temperature at T_2 ;
 T_g = transition temperature;
 T_{ref} = reference temperature;
 T_0 = initial temperature;
 T_1-T_2 = temperature step;
 t^* = intrinsic time;
 t_f = life time;
V = instantaneous specific volume;
 $V_{0,2}$ = volume just after temperature change;
 $V_{\infty,2}$ = equilibrium volume at T_2 ;
 w_{ij} = weights in relaxation functions expanded into Prony series;
Y = shape factor;
 β = instantaneous thermal expansion coefficient;
 β_g = thermal expansion coefficient of solid glass;
 β_l = thermal expansion coefficient of liquid glass;
 ξ = reduced time;
 λ = thermal conductivity;
 λ_i = structural relaxation times;
 σ = applied bending stress;
 σ_i = strength in inert medium;
 σ_u = threshold stress ($P_f = 0$);
 σ_0 = apparent Weibull stress;
 σ_0^* = intrinsic Weibull stress;
 τ_{ij} = relaxation times in relaxation functions expanded into Prony series; and
 Ψ_i = relaxation functions.